

Negative Thermal Expansion of Carbon Nanotube Bundles

Leysan Kh. Galiakhmetova, Elena A. Korznikova,* Aleksey A. Kudreyko,
and Sergey V. Dmitriev

A bundle of aligned carbon nanotubes (CNTs) under lateral loading and heating is considered under plane strain conditions within the framework of a molecular dynamics model with a reduced number of degrees of freedom. Bundles of CNTs of sufficiently large diameter exhibit negative lateral thermal expansion. The coefficient of thermal expansion is practically constant up to a temperature of 1500 K and practically does not depend on biaxial lateral compression up to a volumetric compressive strain of 0.06. This anomalous behavior is explained by the two mechanisms: elliptization of the CNT cross section and bending of the CNT walls by thermal fluctuations. Elliptization leads to a decrease in the cross-sectional area of the CNT, and the bending of the CNT wall leads to a decrease in the effective diameter of the CNT. A bundle with CNTs of the largest investigated diameter demonstrates a large negative coefficient of linear thermal expansion, $\alpha \approx -10^{-4} \text{ K}^{-1}$, which is weakly dependent on temperature.

of negative thermal expansion have been described,^[1–8] including transverse vibrations of 2D materials^[9] or the presence of low-frequency vibrational modes of structural units with rotational degrees of freedom,^[10] phase transitions,^[11] and chemical modifications.^[12,13] Metal nanowires can exhibit negative thermal expansion (NTE) due to elastic softening, as well as due to the effect of surface stress.^[14] A negative CTE can appear as a result of a decrease in the size of nanoparticles caused by internal surface pressure.^[15]

Various mechanisms for the realization of NTE are described in the review;^[16] some are associated with transverse acoustic modes, while others with the rotation of rigid polyhedral groups of atoms.

Thermal expansion can be anisotropic, so that a negative CTE can appear along a certain direction, and a positive one in an orthogonal direction.^[17] Measurements of CTE for nanographite have shown that reducing the size of the graphite domain lowers the temperature at which the thermal expansion along the in-plane direction changes from negative to positive, and this can be explained by the suppression of the out-of-plane vibration.^[18]

In recent years, carbon nanomaterials such as carbon nanotubes (CNTs)^[19,20] and graphene^[21,22] have received a lot of attention from researchers because they exhibit a combination of properties that make them useful in nanotechnologies. The effect of hydrostatic pressure on structure and mechanical properties of chiral CNTs was analyzed by Imtani and Jindal.^[23,24] Following graphene, a large number of other 2D nanomaterials^[25] were discovered and studied, and, as it turned out, 2D materials very often exhibit NTE. This has been demonstrated for graphene,^[26,27] graphyne,^[28] 2D nitrides,^[29] arsenene and antimonene,^[30] transition metal dichalcogenides,^[31,32] phosphorene,^[33–35] and layered van der Waals structures.^[36] Using the molecular dynamics method, it was shown that origami structures made of graphene can have both positive and negative thermal expansion coefficients, depending on the structure.^[37]

First-principles simulations showed that the NTE in 2D materials is determined by the out-of-plane ZA phonon modes, which have a negative Grüneisen parameter.^[28] Out-of-plane bending of membrane-like materials results in in-plane shrinkage as the temperature rises.^[27,38–40] Single-layer graphene can demonstrate NTE at temperatures above 2300 K due to the high-frequency optical ZO mode with a small negative Grüneisen parameter.^[27,38] The effect of doping with B and N on the NTE of graphene was considered in a first-principles study.^[41] It was shown that pure

1. Introduction

Most materials increase in size when heated, that is, they have a positive coefficient of thermal expansion (CTE). CTE is one of the most important characteristics of materials, widely used in engineering calculations. The positiveness of the CTE is explained by the asymmetry of the potentials of interatomic interactions, which is observed for chemical bonds of any type. A negative coefficient of thermal expansion can appear only in materials with a special structure that compensates for the asymmetry of interatomic interactions. In the literature, various mechanisms for the appearance

L. K. Galiakhmetova, S. V. Dmitriev
Institute for Metals Superplasticity Problems
RAS
Ufa 450001, Russia

L. K. Galiakhmetova, S. V. Dmitriev
Institute of Molecule and Crystal Physics
Ufa Federal Research Center
RAS
Ufa 450054, Russia

E. A. Korznikova
Ufa State Petroleum Technological University
Ufa 450000, Russia
E-mail: elena.a.korznikova@gmail.com

A. A. Kudreyko
Department of Medical Physics and Informatics
Bashkir State Medical University
Ufa 450008, Russia

 The ORCID identification number(s) for the author(s) of this article can be found under <https://doi.org/10.1002/pssr.202100415>.

DOI: 10.1002/pssr.202100415

graphene exhibits NTE over the entire investigated temperature range (up to 1000 K) and that doping increases the negativity of the Grüneisen parameter. The implicit frequency shift was calculated for different modes in a pure graphene sheet using the first-principles approach,^[42] and it was shown that the frequency shift is large negative for the ZA and ZO modes, and the negativity of the shift increases with increasing temperature.

The deposition of a thin aluminum film on highly aligned CNT microcantilevers reinforced with ceramic interlocking allows the formation of bimaterial actuators.^[43] It was confirmed experimentally that individual CNTs have a negative radial CTE.^[44,45] Due to the van der Waals forces, CNTs can form aligned arrays called bundles.^[46–49] They have excellent mechanical properties and can be used to make super-strong yarns and ropes.^[50–52] A linear relationship was demonstrated between the axial strength of CNT bundles and the length distribution of CNTs.^[53]

It is interesting to study CNT bundles under lateral loading, when they can be analyzed under plane strain conditions. To effectively solve these problems, the model of a chain moving on a plane^[54–57] was modified to analyze the mechanical response of the CNT bundle cross section subjected to transverse loading and heating.^[58–61]

In this work, using molecular dynamics within the framework of the model of a chain moving on a plane, we calculate the dependence of pressure on temperature in a CNT bundle subjected to biaxial compression. It was unexpectedly found that at a constant volume, the pressure decreases with increasing temperature, which means negative thermal expansion of the CNT bundle.

2. Simulation Details

In this work, single-walled zigzag CNTs of the same diameter are considered under plane strain conditions, which means that the axial deformation of CNTs is equal to zero and the problem becomes 2D. The axial deformation of CNTs can be neglected in our simulations because the most important contribution to the observed effects comes from CNT wall bending rather than from its circumferential and axial strain. The latter ones are much smaller because the bending stiffness of CNT wall is orders of magnitude smaller than the tensile stiffness. Graphene is elastically isotropic; at not very large bending, its bending stiffness weakly depends on the bending direction and therefore on CNT chirality. CNT cross sections create in the x, y plane a densely packed structure, as shown in **Figure 1**. Periodic boundary conditions are applied in two directions. Computational cell contains 12 rows of CNTs along y axis and 10 CNTs along x . Total number of CNTs is 120.

The interatomic distance in the CNT wall is $\rho = 1.418 \text{ \AA}$. Then the distance between the nearest carbon atoms, in projection onto the x, y plane, is equal to $a = \rho\sqrt{3}/2$. CNT cross section is presented by an even number of carbon atoms N_c . Each atom is a member of a rigid atomic chain normal to the x, y plane. CNT diameter is $D = a/\sin(\pi/N_c)$. For N_c much greater than π , $D = aN_c/\pi$. The equilibrium distance between the walls of neighboring CNTs, d , is found as a result of structure relaxation at zero temperature. The distance between the centers of neighboring CNTs is $A = D + d$.

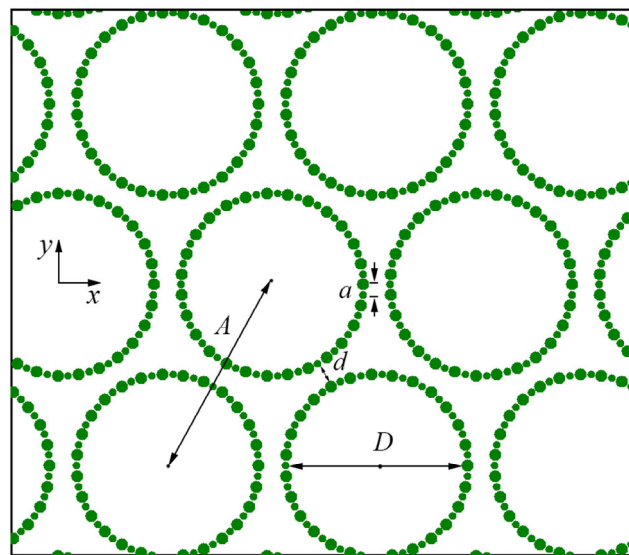


Figure 1. Geometry of the CNT bundle under plain strain conditions. CNTs have zigzag chirality ($m,0$). CNT cross sections create a close packed molecular crystal. Each carbon atom represents a rigid chain of atoms normal to the x, y plane. Atoms moving on the x, y plane have two degrees of freedom. Two sets of chains shifted with respect to each other along z axis are plotted by smaller and larger dots. Distance between nearest chains is a , distance between walls of nearest CNTs is d , CNT diameter is D , and the distance between centers of neighboring CNTs is $A = d + D$.

To study the effect of CNT diameter, we consider the bundles of CNTs with $N_c = 18, 30, 42, 54, 66,$ and 72 . In **Figure 1**, a part of the computational cell is shown for the case of $N_c = 54$. Total number of atoms in the computational cell is $L = 120 N_c$. **Table 1** shows the initial parameters of the CNTs and computational cells: CNT diameter, distance between the centers of CNTs, and the total number of atoms.

The total energy of the system is described by the Hamiltonian, which includes four terms

$$H = K + E_B + E_A + E_{vdW} \quad (1)$$

here K is the kinetic energy; E_B and E_A give the energy of valence bonds and valence angles, respectively. The E_{vdW} term describes the energy of van der Waals interactions. A detailed formulation of the model and description of the model parameters can be found in the work.^[59] The model has been successfully used to describe structure and peculiar mechanical properties of CNT bundles and other carbon 2D materials. In particular, it was used to model folded and scrolled configurations of graphene nanoribbons,^[54,56] dynamics of surface ripplications^[55]

Table 1. Geometrical parameters of the CNTs and computational cells used in simulations.

Number of atoms in CNT cross section, N_c	18	30	42	54	66	78
CNT diameter, D [Å]	7.07	11.7	16.4	21.1	25.8	30.5
Distance between CNT centers, A [Å]	10.15	14.83	19.5	24.2	25.8	33.57
Total number of atoms, L	2160	3600	5040	6480	7920	9360

and rotobreathers,^[62] graphene winding around carbon nanotube,^[57] mechanical response of CNT bundle to lateral compression,^[58,59,61] damping properties of CNT bundles,^[60] partial auxeticity of laterally compressed CNT bundles,^[63] and natural bending frequencies of CNTs.^[64] The calculated natural frequencies are in a good agreement with the experimental data.^[65] Full-atomic modeling has confirmed that the chain model correctly reproduces natural frequencies of bending oscillations of CNTs, scrolls and folds of graphene nanoribbons, and shows good results in solving other problems where bending is the main deformation mode.^[54–56]

The Euler–Lagrange equations of motion can be derived from the Hamiltonian (1) using the Hamilton’s principle. The equations of motion are integrated with the use of the Störmer method of order six with the time step of 0.1 fs.

The simulation included the following steps: 1) a simulation cell with idealized structure composed of circular CNT cross sections is created, as shown in Figure 1; 2) the structure is then relaxed at zero temperature and zero pressure; 3) the relaxed structure is subjected to biaxial compression, $\epsilon_{xx} = \epsilon_{yy}$, at four values of volumetric deformation $\theta = \epsilon_{xx} + \epsilon_{yy} = 0.0, -0.02, -0.04,$ and -0.06 ; and (4) at the last step, a temperature is applied to the compressed structure at a rate of 7.5 K ps^{-1} . This heating rate is slow enough that a further decrease in the heating rate does not appreciably affect the results. During heating, the volume and shape of the computational cell do not change.

The mechanical properties of CNT bundles considered here are given in the study by Korznikova et al.^[63] In particular, for the case of CNT with 30 carbon atoms in its cross section, Young’s and shear moduli are 110 and 30 MPa, respectively, and Poisson’s ratio is 0.83.

3. Numerical Results

Calculations are performed for six structures with different CNT diameters and for four values of the volumetric compressive strain $|\theta|$. For each case, the dependence of pressure on temperature is calculated in the range $T \leq 1500 \text{ K}$ and shown in **Figure 2**. For CNTs of smallest diameter, $N_c = 18$, shown in Figure 2a, pressure increases with temperature up to $T = 500 \text{ K}$ and then remains nearly constant. An increase in the compressive strain value leads to an increase in pressure. In the case of $N_c = 30$, shown in Figure 2b, the pressure also increases with increasing $|\theta|$, but it decreases with temperature, and this decrease occurs faster at higher values of biaxial compression. Note that the decrease in pressure with temperature observed in our simulations at constant volume means that the CNT bundle exhibits negative thermal expansion. For the largest investigated CNT diameter, see panel Figure 2f, $p(T)$ becomes practically independent of the magnitude of the compressive strain, and negative CTE is observed over the entire investigated temperature range. It can also be seen from Figure 2f that for nonzero values of $|\theta|$, the pressure drops with temperature very quickly in the interval $T < 50 \text{ K}$, and then decreases almost linearly with a rate practically independent of $|\theta|$. For intermediate values of the CNT diameter, see Figure 2, panels (c)–(e), for small $|\theta|$ pressure decreases linearly with temperature and increases with increasing

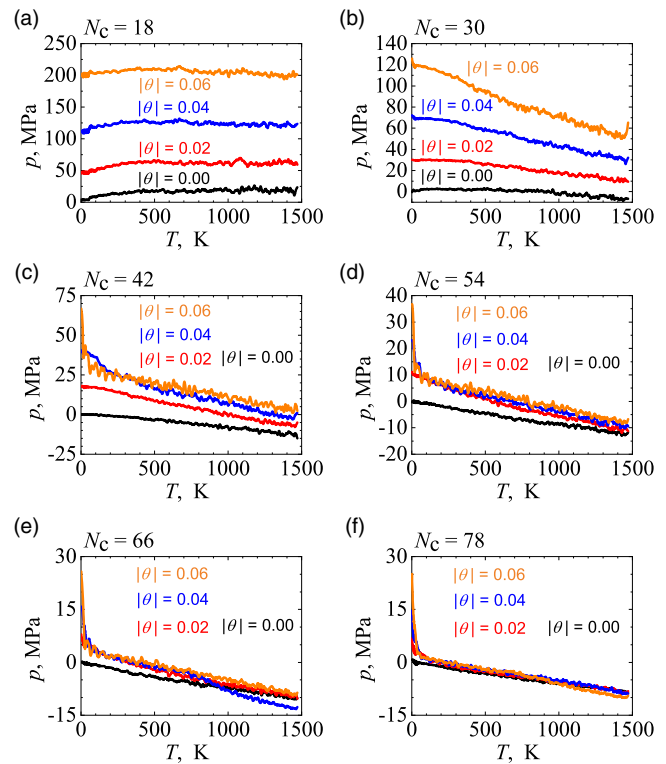


Figure 2. Pressure versus temperature plots for different degrees of volumetric deformation at different CNT diameters.

$|\theta|$. However, for larger $|\theta|$, at the beginning of heating, a rapid drop in pressure is observed and the dependence of the $p(t)$ curve on $|\theta|$ disappears. All these features of the $p(T)$ curves will become clear after analyzing the structural transformations in CNT bundles of different diameters.

Let us describe in detail the structure of the CNT bundle in the case $N_c = 54$ ($D = 21.1 \text{ \AA}$), see Figure 2d, because in this case the $p(T)$ curves for $|\theta| = 0.0$ and 0.02 qualitatively differ from the curves for $|\theta| = 0.04$ and 0.06 . In the first case, p decreases linearly with increasing T , and the curve for $|\theta| = 0.0$ lies below the curve corresponding to $|\theta| = 0.02$, while in the second case, at the beginning of heating, one can see a rapid decrease in p and the dependence on $|\theta|$ disappears.

The rapid decrease in some of the $p(T)$ curves at the beginning of heating (see Figure 2) is due to the elliptization of CNTs. The CNT cross section can be characterized by the degree of ellipticity, which can be defined as the ratio of the minimum diameter of the CNT to the maximum diameter, D_{\min}/D_{\max} . In **Figure 3**, for the case of $N_c = 54$, time evolution of the histogram of the CNT ellipticity is shown for the CNT bundle under volumetric compressive strain $|\theta|$ equal to (a) 0.0, (b) 0.02, (c) 0.04, and (d) 0.06. The ordinate shows the number of CNTs, n , with a certain ratio D_{\min}/D_{\max} (note that there are 120 CNTs in the computational cell). Curves of different colors represent histograms at times from 1 to 7 ps with a step of 1 ps. Recall that the heating rate is 7.5 K ps^{-1} , so that at $t = 7 \text{ ps}$ the temperature reaches 52.5 K .

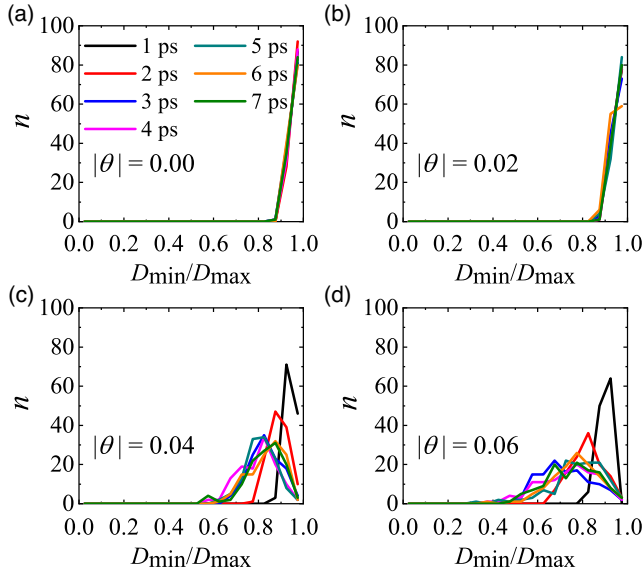


Figure 3. a–d) Time evolution of the histogram of the CNT elliptization parameter D_{\min}/D_{\max} in a CNT bundle with $N_c = 54$ for biaxial volumetric compressive strain $|\theta|$ equal to 0.0 (a), 0.02 (b), 0.04 (c), and 0.06 (d). The ordinate shows the number of CNTs, n , with a certain ratio D_{\min}/D_{\max} (note that there are 120 CNTs in the computational cell). Curves of different colors, as shown in (a), give results at times from 1 to 7 ps with a step of 1 ps.

As follows from Figure 3, for $|\theta| = 0.0$ and 0.02 histograms do not change over time and have single maximum near $D_{\min}/D_{\max} = 1$, see (a) and (b). This means that at low values of the compressive strain, the cross sections of CNTs remain almost circular. The situation is qualitatively different for $|\theta| \geq 0.04$, see (c) and (d). Structures with circular CNTs become unstable and elliptization of CNTs takes place. By the time $t = 52.5$ ps, the structure transformation is complete, and the maximum of the D_{\min}/D_{\max} histogram shifts to about 0.8 in (c) and 0.7 in (d). During this structure transformation a fast drop of pressure is observed in Figure 2d for $|\theta| = 0.04$ and 0.06. Pressure in the CNT bundles composed of CNTs with noncircular cross sections is practically independent on the volumetric compressive strain, as it was reported in the work.^[59,60] For this reason, the $p(T)$ curves in structures with noncircular CNTs are independent of $|\theta|$ (see Figure 2f).

Structure of the bundle composed of CNTs with $N_c = 54$ at different values of compressive strain $|\theta|$ and different temperatures can be seen in Figure 4. From the first column of Figure 4, which corresponds to $T = 50$ K, it is clearly seen that at $|\theta| = 0.0$ and 0.02 CNTs have nearly circular cross sections but for $|\theta| = 0.04$ and 0.06 CNTs are elliptic. As the temperature rises, the structures become less regular, and this tendency is more pronounced for greater compressive strain $|\theta|$.

As mentioned in Section 1, the in-plane NTE of 2D materials is explained by lateral thermal fluctuations (excitation of phonon ZA modes), which lead to in-plane shrinkage.^[27,28,38–40] This mechanism should also work for CNT bundles due to a decrease in the effective diameter of CNTs owing to bending of the CNT walls due to thermal fluctuations. To test this assumption, the average CNT diameter is calculated as follows

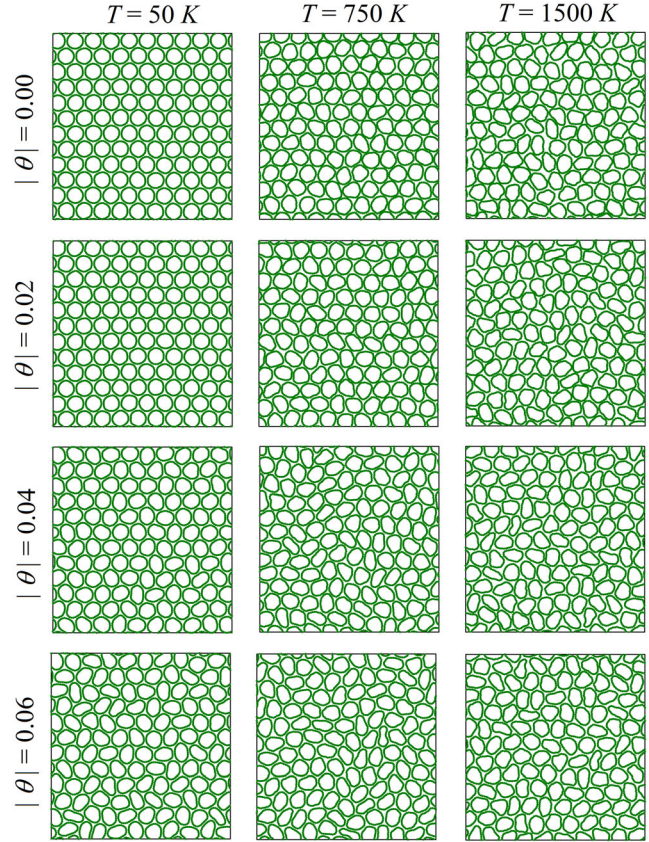


Figure 4. Structure of the bundle composed of CNTs with $N_c = 54$ at different values of compressive strain $|\theta|$ and different temperatures.

$$\langle D \rangle = \frac{2}{JN_c} \sum_j \sum_n^{N_c/2} (|r_{j,n} - r_{j,n+N_c/2}|) \quad (2)$$

where the averaging is performed over all J CNTs in the computational cell and over half of the atoms in each CNT cross section.

In Figure 5, the temperature dependence of the averaged diameter of CNTs in the bundle with $N_c = 54$ is shown for four values of compressive strain (indicated for each curve). The averaged CNT diameter is normalized to the equilibrium diameter $D_0 = 21.03$ Å. This result confirms that the average diameter of CNTs decreases with temperature, explaining the observed NTE effect.

Elliptization of CNT cross sections upon heating and/or biaxial compression can be another mechanism for NTE. To demonstrate this, we calculate the cross-sectional area of circular and elliptic CNTs under the condition that their perimeters are equal, which is ensured by the high tensile stiffness of the CNT wall. A circular cross section of radius R has an area $S_c = \pi R^2$ and an elliptic cross section has an area $S_e = \pi ab$, where a and b are the major and minor axes, respectively. Perimeter of the circle is $C_c = 2\pi R$ and the perimeter of the ellipse can be calculated with the use of the Ramanujan's approximate formula $C_e = \pi[3(a+b) - \sqrt{(3a+b)(a+3b)}]$. This formula is very accurate for ellipses with not too large eccentricity. From the condition $C_c = C_e$ one finds

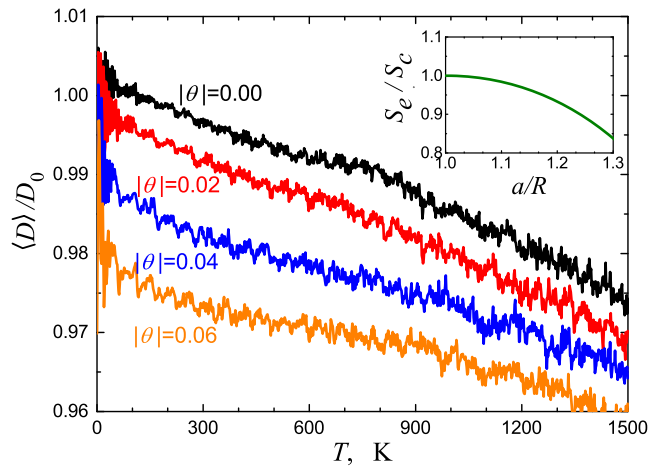


Figure 5. Dependence of the average diameter of CNTs on temperature for a bundle consisting of CNTs with $N_c = 54$ at different values of compressive strain $|\theta|$. The averaged CNT diameter is normalized to the equilibrium diameter $D_0 = 21.03 \text{ \AA}$. The inset shows the ratio of the areas of the elliptical cross section to the circular cross section of CNTs depending on the ratio a/R , which characterizes the degree of elliptization.

$$b = -\frac{2}{3}a + R + \frac{1}{3}\sqrt{3R^2 + 6aR - 5a^2} \quad (3)$$

and using this expression, we find the ratio of the area of the ellipse to the area of the circle

$$\frac{S_e}{S_c} = -\frac{2}{3}\xi^2 + \xi + \frac{1}{3}\xi\sqrt{3 + 6\xi - 5\xi^2}, \quad \xi = \frac{a}{R} \geq 1 \quad (4)$$

The inset of Figure 5 shows the ratio S_e/S_c as a function of the ratio a/R (see Equation (4)). It can be seen that the elliptization of CNTs leads to a decrease in the cross-sectional area. This means that the elliptization of CNTs contributes to the effect of NTE.

Finally, we estimate the CTE for the case $N_c = 78$ ($D = 30.5 \text{ \AA}$) and $|\theta| = 0.0$ at two temperatures: $T = 500$ and 1000 K . For this purpose, we maintain a constant temperature and gradually increase the compressive strain until the negative pressure reaches zero. It is found that at $T = 500 \text{ K}$ the pressure becomes zero at $\epsilon_{xx} = \epsilon_{yy} = -0.044$ and for $T = 1000 \text{ K}$ at $\epsilon_{xx} = \epsilon_{yy} = -0.097$. Therefore, it turns out that the coefficient of linear thermal expansion at $T = 500 \text{ K}$ is equal to $\alpha = -8.8 \times 10^{-5} \text{ K}^{-1}$ and at $T = 1000 \text{ K}$ is equal to $\alpha = -9.7 \times 10^{-5} \text{ K}^{-1}$. We conclude that the CNT bundle exhibits a strongly negative CTE, which is weakly dependent on temperature.

4. Discussion and Conclusions

The pressure–temperature curves were calculated for CNT bundles considered under plane strain conditions at constant volume using the molecular dynamics method based on a chain model with a reduced number of degrees of freedom. The influence of the CNT diameter ($7.07 \leq D \leq 30.5 \text{ \AA}$) and biaxial compressive strain ($0 \leq |\theta| \leq 0.06$) on the $p(T)$ curves was analyzed within the temperature range $0 \leq T \leq 1500 \text{ K}$.

It was found that in the bundles of CNTs of relatively small diameter, $N_c \leq 30$ ($D \leq 11.7 \text{ \AA}$), pressure increases with compressive strain, while in the case of CNTs of large diameter, $N_c = 78$ ($D = 30.5 \text{ \AA}$), curves $p(T)$ are independent of biaxial compressive strain. Small diameter CNTs under moderate biaxial compression retain an almost circular cross sections, but large diameter CNTs under biaxial compression acquire elliptical cross sections, for which, as demonstrated in previous studies,^[59,60] volumetric compression occurs at almost constant pressure.

In CNT bundles with CNT diameter $D \geq 16.4 \text{ \AA}$, the pressure decreases with increasing temperature at a constant volume (see Figure 2), which means a negative CTE value. CNTs of small diameter have a positive or nearly zero CTE.

The negative CTE can be realized through two mechanisms. First is the bending of the CNT walls by thermal vibrations, which effectively reduce the CNT diameter (see Figure 5). This is similar to the in-plane shrinkage effect of 2D materials due to thermally induced out-of-plane displacements.^[27,38–40] Second is CNT elliptization, which leads to the reduction of the CNT cross-sectional area (see the inset of Figure 5). For CNTs of small diameter, these effects are small because of their high bending stiffness.

The estimation of CTE for the case of $D = 30.5 \text{ \AA}$ gave rather large negative values $\alpha = -8.8 \times 10^{-5} \text{ K}^{-1}$ for $T = 500 \text{ K}$ and $-9.7 \times 10^{-5} \text{ K}^{-1}$ for $T = 1000 \text{ K}$. Dependence of α on temperature is weak. Note that a large positive CTE value was observed when simulating the winding of a graphene nanoribbon around CNT,^[57] and large negative and positive CTE values can be achieved by changing the structure of the graphene origami.^[37]

The large negative coefficient of thermal expansion of CNT bundles, which weakly depends on temperature, makes it possible to propose their use for the development of temperature sensors operating in a wide temperature range.

The geometry of CNTs strongly affects the thermomechanical properties of materials based on them;^[66] therefore, in future studies, the CTE will be calculated for beams of multiwalled CNTs. Nanotubes can be formed from a variety of 2D materials,^[67,68] and it would be interesting to develop a chain model suitable for modeling them under plane deformation conditions, which is also included in the future work plan. The influence of surface functional groups or impurities should be considered in future studies because they can significantly affect the thermomechanical properties of CNT bundles.^[41]

Acknowledgements

L.K.G. and S.V.D. acknowledge the financial support of the Russian Science Foundation grant no. 21-12-00229.

Conflict of Interest

The authors declare no conflict of interest.

Data Availability Statement

Research data are not shared.

Keywords

carbon nanotube bundles, chain model, lateral compression, molecular dynamics, negative thermal expansion

Received: July 29, 2021

Revised: October 1, 2021

Published online:

- [1] E. Liang, Q. Sun, H. Yuan, J. Wang, G. Zeng, Q. Gao, *Front. Phys.* **2021**, *16*, 53302.
- [2] Z. Cheng, M. Zhou, B. Yang, R. Zhen, *Cailiao Daobao/Mater. Rep.* **2020**, *34*, 9095.
- [3] R. Mittal, M. K. Gupta, S. L. Chaplot, *Prog. Mater. Sci.* **2018**, *92*, 360.
- [4] K. Takenaka, *Front. Chem.* **2018**, *6*, <https://doi.org/10.3389/fchem.2018.00267>.
- [5] C. Lind, *Materials* **2012**, *5*, 1125.
- [6] K. Takenaka, *Sci. Technol. Adv. Mater.* **2012**, *13*, 013001.
- [7] W. Miller, C. W. Smith, D. S. MacKenzie, K. E. Evans, *J. Mater. Sci.* **2009**, *44*, 5441.
- [8] G. D. Barrera, J. A. O. Bruno, T. H. K. Barron, N. L. Allan, *J. Phys. Condens. Mater.* **2005**, *17*, R217.
- [9] V. A. Kuzkin, A. M. Krivosov, *Phys. Status Solidi B* **2015**, *252*, 1664.
- [10] X. Cheng, J. Yuan, X. Zhu, K. Yang, M. Liu, Z. Qi, *J. Phys. D: Appl. Phys.* **2018**, *51*, 095303.
- [11] M. Azuma, Y. Sakai, T. Nishikubo, K. Oka, H. Yamamoto, *Rev. High Pressure Sci. Technol./Koatsuryoku No Kagaku To Gijutsu* **2020**, *30*, 187.
- [12] J. Chen, L. Hu, J. Deng, X. Xing, *Chem. Soc. Rev.* **2015**, *44*, 3522.
- [13] J. H. He, *Rep. Mech. Eng.* **2020**, *1*, 187.
- [14] D. T. Ho, S. Y. Kwon, H. S. Park, S. Y. Kim, *Nano Lett.* **2017**, *17*, 5113.
- [15] J. H. Belo, A. L. Pires, I. T. Gomes, V. Andrade, J. B. Sousa, R. L. Hadimani, D. C. Jiles, Y. Ren, X. Zhang, J. P. Araújo, A. M. Pereira, *Phys. Rev. B* **2019**, *100*, 134303.
- [16] K. W. Wojciechowski, F. Scarpa, J. N. Grima, A. Alderson, *Phys. Status Solidi B* **2015**, *252*, 1421.
- [17] J. N. Grima, P. S. Farrugia, R. Gatt, V. Zammit, *Proc. R. Soc. A: Math. Phys.* **2007**, *463*, 1585.
- [18] K. Akikubo, T. Kurahashi, S. Kawaguchi, M. Tachibana, *Carbon* **2020**, *169*, 307.
- [19] S. Iijima, *Nature* **1991**, *354*, 56.
- [20] I. Evazzade, I. P. Lobzenko, O. Golubev, E. A. Korznikova, *J. Micromech. Mol. Phys.* **2020**, *5*, 2050001.
- [21] K. S. Novoselov, A. K. Geim, S. V. Morozov, D. Jiang, M. I. Katsnelson, I. V. Grigorieva, S. V. Dubonos, A. A. Firsov, *Nature* **2005**, *438*, 197.
- [22] T. Yoon, S. Kang, T. Y. Kang, T.-S. Kim, *Comput. Model. Eng. Sci.* **2019**, *120*, 351.
- [23] A. N. Imtani, V. K. Jindal, *Carbon* **2009**, *47*, 3247.
- [24] A. N. Imtani, V. K. Jindal, *Comput. Mater. Sci.* **2009**, *46*, 297.
- [25] B. Liu, K. Zhou, *Prog. Mater. Sci.* **2019**, *100*, 99.
- [26] D. Yoon, Y.-W. Son, H. Cheong, *Nano Lett.* **2011**, *11*, 3227.
- [27] C. P. Romao, *Phys. Rev. B* **2017**, *96*, 134113.
- [28] C.-W. Kim, S.-H. Kang, Y.-K. Kwon, *Phys. Rev. B* **2015**, *92*, 245434.
- [29] I. Demiroglu, C. Sevik, *Phys. Rev. B* **2021**, *103*, 085430.
- [30] G. Liu, J. Zhou, *J. Phys. Condens. Mater.* **2019**, *31*, 065302.
- [31] Z.-Y. Wang, Y.-L. Zhou, X.-Q. Wang, F. Wang, Q. Sun, Z.-X. Guo, Y. Jia, *Chin. Phys. B* **2015**, *24*, 026501.
- [32] D. Kumar, B. Singh, P. Kumar, V. Balakrishnan, P. Kumar, *J. Phys. Condens. Mater.* **2019**, *31*, 505403.
- [33] H. Sun, G. Liu, Q. Li, X. G. Wan, *Phys. Lett. A* **2016**, *380*, 2098.
- [34] L. Wang, C. Wang, Y. Chen, *J. Phys. Condens. Mater.* **2019**, *31*, 465003.
- [35] B. Liu, L. Bai, E. A. Korznikova, S. V. Dmitriev, A. W.-K. Law, K. Zhou, *J. Phys. Chem. C* **2017**, *121*, 13876.
- [36] A. M. Chippindale, S. J. Hibble, E. Marelli, E. J. Bilbe, A. C. Hannon, M. Zbiri, *Dalton Trans.* **2015**, *44*, 12502.
- [37] D. T. Ho, H. S. Park, S. Y. Kim, U. Schwingenschlögl, *ACS Nano* **2020**, *14*, 8969.
- [38] Y. Hu, J. Chen, B. Wang, *Carbon* **2015**, *95*, 239.
- [39] J. A. Baimova, S. V. Dmitriev, K. Zhou, *Phys. Status Solidi B* **2012**, *249*, 1393.
- [40] E. Randjbaran, D. L. Majid, R. Zahari, M. T. H. Sultan, N. Mazlan, *Facta Universitatis, Ser. Mech. Eng.* **2020**, *18*, 229.
- [41] S. Mann, R. Kumar, V. K. Jindal, *RSC Adv.* **2017**, *7*, 22378.
- [42] S. Mann, V. K. Jindal, *Mater. Res. Express* **2017**, *4*, 075038.
- [43] P. Zhang, J. Guo, H. Hou, Y. Zhang, X. Yang, H. Zhong, L. Chen, Y. Zhao, *ChemNanoMat* **2020**, *6*, 404.
- [44] A. V. Dolbin, V. B. Esel'Son, V. G. Gavrilko, V. G. Manzhelii, S. N. Popov, N. A. Vinnikov, N. I. Danilenko, B. Sundqvist, *Low Temp. Phys.* **2009**, *35*, 484.
- [45] A. Koochi, M. Goharimanesh, *Rep. Mech. Eng.* **2021**, *2*, 41.
- [46] B. C. Liu, T. J. Lee, S. H. Lee, C. Y. Park, C. J. Lee, *Chem. Phys. Lett.* **2003**, *377*, 55.
- [47] Y. Li, X. B. Zhang, X. Y. Tao, J. M. Xu, W. Z. Huang, J. H. Luo, Z. Q. Luo, T. Li, F. Liu, Y. Bao, H. J. Geise, *Carbon* **2005**, *43*, 295.
- [48] R. Zhang, Q. Wen, W. Qian, D. S. Su, Q. Zhang, F. Wei, *Adv. Mater.* **2011**, *23*, 3387.
- [49] E. G. Rakov, *Russ. Chem. Rev.* **2013**, *82*, 538.
- [50] Y. Bai, R. Zhang, X. Ye, Z. Zhu, H. Xie, B. Shen, D. Cai, B. Liu, C. Zhang, Z. Jia, S. Zhang, X. Li, F. Wei, *Nat. Nanotechnol.* **2018**, *13*, 589.
- [51] J. Di, S. Fang, F. A. Moura, D. S. Galvão, J. Bykova, A. Aliev, M. J. D. Andrade, X. Lepró, N. Li, C. Haines, R. Ovalle-Robles, D. Qian, R. H. Baughman, *Adv. Mater.* **2016**, *28*, 6598.
- [52] D. Appell, *Phys. World* **2011**, *24*, 30.
- [53] N. Gupta, J. M. Alred, E. S. Penev, B. I. Yakobson, *ACS Nano* **2021**, *15*, 1342.
- [54] A. V. Savin, E. A. Korznikova, S. V. Dmitriev, *Phys. Solid State* **2015**, *57*, 2348.
- [55] A. V. Savin, E. A. Korznikova, S. V. Dmitriev, *Phys. Rev. B* **2019**, *99*, 235411.
- [56] A. V. Savin, M. A. Mazo, *Phys. Solid State* **2018**, *60*, 826.
- [57] A. Savin, E. Korznikova, S. Dmitriev, E. Soboleva, *Comput. Mater. Sci.* **2017**, *135*, 99.
- [58] E. Korznikova, L. Rysaeva, A. Savin, E. Soboleva, E. Ekomasov, M. Ilgamov, S. Dmitriev, *Materials* **2019**, *12*, 3951.
- [59] D. U. Abdullina, E. A. Korznikova, V. I. Dubinko, D. V. Laptev, A. A. Kudreyko, E. G. Soboleva, S. V. Dmitriev, K. Zhou, *Computation* **2020**, *8*, 27.
- [60] L. K. Rysaeva, E. A. Korznikova, R. T. Murzaev, D. U. Abdullina, A. A. Kudreyko, J. A. Baimova, D. S. Lisovenko, S. V. Dmitriev, *Facta Universitatis, Ser.: Mech. Eng.* **2020**, *18*, 1.
- [61] L. K. Rysaeva, D. V. Bachurin, R. T. Murzaev, D. U. Abdullina, E. A. Korznikova, R. R. Mulyukov, S. V. Dmitriev, *Facta Universitatis, Ser.: Mech. Eng.* **2020**, *18*, 525.
- [62] S. V. Dmitriev, A. S. Semenov, A. V. Savin, M. A. Ilgamov, D. V. Bachurin, *J. Micromech. Mol. Phys.* **2020**, *5*, 2050010.
- [63] E. A. Korznikova, K. Zhou, L. K. Galiakhmetova, E. G. Soboleva, A. A. Kudreyko, S. V. Dmitriev, *Phys. Status Solidi RRL* **2021**, *2021*, 2100189.
- [64] S. V. Dmitriev, I. R. Sunagatova, M. A. Ilgamov, I. S. Pavlov, *Tech. Phys.* **2021**, *91*, 189.
- [65] C.-Y. Li, T.-W. Chou, *Nanotechnology* **2004**, *15*, 1493.
- [66] O. Aluko, S. Gowtham, G. Odegard, *J. Micromech. Mol. Phys.* **2020**, *5*, 2050005.
- [67] S. Shcherbinin, S. Ustuzhanina, A. Kistanov, *J. Micromech. Mol. Phys.* **2020**, *5*, 2050007.
- [68] S. A. Shcherbinin, K. Zhou, S. V. Dmitriev, E. A. Korznikova, A. R. Davletshin, A. A. Kistanov, *J. Phys. Chem. C* **2020**, *124*, 10235.